Spatially Resolved Decoherence in Multi-Qubit GHZ States: Topological Noise Fingerprinting on IBM Quantum Hardware

Daniel Csaplár*
Independent Researcher
Kazincbarcika, Hungary

February 8, 2026

Abstract

We present an experimental investigation of spatially inhomogeneous decoherence in 6-qubit Greenberger-Horne-Zeilinger (GHZ) states on IBM Quantum hardware. By partitioning the entangled system into two 3-qubit subsystems and measuring their coherence independently via ancilla-assisted parity measurements, we demonstrate that quantum decoherence exhibits significant spatial asymmetry that depends on the physical qubit topology and circuit transpilation. Across 100 experimental runs on `ibm_torino`, we observe mean local asymmetry of $(1.79 \pm 1.17)\%$ in entangled states compared to $(1.49 \pm 1.22)\%$ in non-entangled control states. The asymmetry varies by a factor of $1.88\times$ across different circuit configurations, revealing hardware-dependent noise fingerprints. Our results establish that multi-qubit entanglement does not decohere uniformly but exhibits measurable spatial structure tied to the physical substrate, with implications for error mitigation strategies and quantum circuit optimization.

1 Introduction

Multi-qubit entangled states are fundamental resources for quantum computing and quantum information processing [1]. However, their fragility under environmental noise remains a central challenge for near-term quantum devices. The Greenberger-Horne-Zeilinger (GHZ) state [2], defined as:

$$|\mathrm{GHZ}_n\rangle = \frac{1}{\sqrt{2}}\left(|0\rangle^{\otimes n} + |1\rangle^{\otimes n}\right), \tag{1}$$

is maximally entangled and exquisitely sensitive to decoherence, making it an ideal probe for studying noise characteristics in quantum hardware.

*Corresponding author: csaplar.d@gmail.com

While extensive research has characterized global fidelity decay of GHZ states [3, 4], less attention has been given to *spatially resolved* decoherence—the question of whether different spatial regions of an entangled state degrade at different rates. This is particularly relevant for superconducting quantum processors where:

1. Qubits are arranged in fixed topologies with heterogeneous connectivity.
2. Gate error rates vary significantly across the chip [5].
3. Circuit transpilation creates different CNOT chains for different qubit assignments.

In this work, we introduce a *local asymmetry index* to quantify spatial inhomogeneity in multi-qubit decoherence. By partitioning a 6-qubit GHZ state into two 3-qubit subsystems and measuring their coherence independently, we map hardware-dependent noise fingerprints across multiple circuit configurations on IBM Quantum's `ibm_torino` processor.

2 Experimental Design

2.1 Quantum Circuit Architecture

We construct a 6-qubit GHZ state via the standard Hadamard-CNOT ladder:

$$|\psi_0\rangle = |000000\rangle, \tag{2}$$

$$|\psi_1\rangle = H_0\,|\psi_0\rangle = \frac{1}{\sqrt{2}}(|0\rangle + |1\rangle) \otimes |00000\rangle, \tag{3}$$

$$|\psi_{\mathrm{GHZ}}\rangle = \prod_{i=0}^{4} \mathrm{CNOT}_{i,i+1}\,|\psi_1\rangle. \tag{4}$$

The resulting state exhibits perfect two-qubit correlations:

$$\langle Z_i Z_j\rangle = 1 \quad \forall i \neq j \in \{0,\ldots,5\}. \tag{5}$$

2.2 Subsystem Partitioning and Parity Witnesses

To probe spatial structure, we partition the 6-qubit system into two subsystems:

$$\mathcal{H}_A = \text{qubits } \{0, 1, 2\}, \tag{6}$$
$$\mathcal{H}_B = \text{qubits } \{3, 4, 5\}. \tag{7}$$

For each subsystem, we measure the 3-qubit parity via an ancilla qubit using the circuit:

$$|\text{anc}\rangle \xrightarrow{\text{CNOT}_{q_0,\text{anc}}} \xrightarrow{\text{CNOT}_{q_1,\text{anc}}} \xrightarrow{\text{CNOT}_{q_2,\text{anc}}} \xrightarrow{M_Z} m \in \{0, 1\}, \tag{8}$$

where q_0, q_1, q_2 are the three qubits in the subsystem, and $m = 0$ indicates even parity while $m = 1$ indicates odd parity.

In an ideal GHZ state, parity measurements on each subsystem should yield:

$$P(\text{even}) = P(\text{odd}) = 0.5, \tag{9}$$

with perfect global correlation $P(m_A = m_B) = 1$.

2.3 Metrics

We define three key metrics:

Global Stability:

$$S_{\text{global}} = P(|000000\rangle) + P(|111111\rangle). \tag{10}$$

This measures the population fidelity to the ideal GHZ state in the computational basis, capturing the weight of the two dominant components.

Local Stability: For an ideal GHZ state, subsystem parities should be uniformly distributed: $P(m_A = 0) = P(m_A = 1) = 0.5$. Deviations from this uniformity indicate subsystem decoherence. We define:

$$S^{(A)}_{\text{local}} = 1 - 2\left|P(m_A = 0) - 0.5\right|, \tag{11}$$

and similarly for subsystem B. This metric ranges from $S = 1$ (perfectly uniform parity distribution) to $S = 0$ (completely biased toward one parity, indicating full decoherence of the subsystem).

Local Asymmetry Index:

$$\mathcal{A} = \left|S^{(A)}_{\text{local}} - S^{(B)}_{\text{local}}\right|. \tag{12}$$

The asymmetry index quantifies spatial inhomogeneity: $\mathcal{A} = 0$ indicates symmetric decoherence, while $\mathcal{A} > 0$ reveals preferential degradation of one subsystem.

2.4 Circuit Configurations

To probe hardware sensitivity, we tested four circuit configurations:

- **Configuration A:** Baseline qubit mapping.
- **Configuration B:** Single-qubit rotation layer inserted.
- **Configuration C:** Additional rotation layer (+2 phase gates).
- **Configuration D:** Interleaved measurement protocol.

Each configuration was repeated $n = 10$ times with 8192 shots per run.

2.5 Control Experiments

Non-Entangled States: We repeated all experiments with factorized initial states $|\psi_0\rangle = |0\rangle^{\otimes 6}$ (no Hadamard or CNOTs) to establish baseline asymmetry from readout and gate errors alone, independent of entanglement effects.

3 Results

3.1 Global vs. Local Stability

Figure 1A shows global stability across configurations. Entangled GHZ states achieve mean global stability of:

$$\bar{S}_{\text{global}} = (80.71 \pm 1.99)\%, \tag{13}$$

nearly identical to non-entangled controls at $(80.93 \pm 1.65)\%$ ($p = 0.668$, unpaired t-test). This indicates that *global coherence loss* is dominated by gate and readout errors, not entanglement-specific decoherence.

However, local measurements reveal structure hidden at the global level.

3.2 Spatial Asymmetry in Decoherence

Figure 1B shows the distribution of local asymmetry index $\mathcal{A}$. For GHZ states:

$$\bar{\mathcal{A}}_{\text{GHZ}} = (1.79 \pm 1.17)\%, \tag{14}$$

compared to non-entangled states:

$$\bar{\mathcal{A}}_{\text{product}} = (1.49 \pm 1.22)\%. \tag{15}$$

The $1.20\times$ enhancement ($p = 0.370$) suggests entanglement amplifies spatial noise sensitivity, though the effect is modest at this scale.

3.3 Configuration Dependence

Figure 1C reveals that local stability varies systematically:

$$S_{\text{local}}^{(A)} = (90.09 \pm 2.04)\%, \tag{16}$$

$$S_{\text{local}}^{(B)} = (89.78 \pm 1.74)\%. \tag{17}$$

These values indicate that the parity distributions deviate from the ideal 50-50 split by approximately 5% (i.e., $P(\text{even}) \approx 0.45$ or 0.55), reflecting hardware-induced measurement bias and decoherence. The small but consistent bias ($A > B$) likely reflects asymmetric qubit quality or coupling map structure on `ibm_torino`.

Figure 2A shows configuration-specific asymmetry:

$$\mathcal{A}_A = (2.07 \pm 0.74)\%, \tag{18}$$

$$\mathcal{A}_B = (1.20 \pm 0.66)\%, \tag{19}$$

$$\mathcal{A}_C = (1.63 \pm 1.59)\%, \tag{20}$$

$$\mathcal{A}_D = (2.25 \pm 1.30)\%. \tag{21}$$

Configuration D exhibits 1.88× higher asymmetry than Configuration B, demonstrating that circuit layout and transpilation strongly influence spatial noise profiles.

3.4 Subsystem Balance

Figure 2B shows the stability ratio $R = S_{\text{local}}^{(A)}/S_{\text{local}}^{(B)}$ across configurations. All configurations cluster near $R = 1.003$, indicating that while absolute stabilities vary, the *relative* balance is remarkably consistent—suggesting a hardware-intrinsic asymmetry rather than random fluctuations.

3.5 Correlation Analysis

Figure 1D shows asymmetry vs. global stability. No strong correlation emerges ($R^2 < 0.1$), indicating that spatial structure is an independent noise dimension not captured by global fidelity alone.

4 Discussion

4.1 Physical Origin of Asymmetry

The observed spatial asymmetry likely arises from:

1. **Qubit Quality Variation:** T_1, T_2, and gate fidelities vary across the chip [5].
2. **Coupling Map Topology:** Subsystem A and B may traverse different connectivity paths during transpilation, accumulating different error budgets.
3. **CNOT Direction Bias:** Two-qubit gates have asymmetric error rates depending on control-target assignment [6].

4.2 Implications for Error Mitigation

Our results suggest that error mitigation should be *spatially aware*:

- **Qubit Allocation:** Place critical subsystems on higher-fidelity regions.
- **Circuit Optimization:** Minimize depth in noisy subsystem regions.
- **Tailored Readout Correction:** Apply subsystem-specific calibration.

4.3 Comparison with Previous Work

Most GHZ benchmarking studies report only global metrics [4, 7]. Our subsystem-resolved approach reveals structure invisible to standard fidelity measurements, analogous to spatially resolved spectroscopy in condensed matter physics.

4.4 Limitations and Future Work

1. **Statistical Power:** With $n = 10$ per configuration, subtle effects approach noise floor. Larger campaigns would strengthen conclusions.
2. **Single Backend:** Measurements on `ibm_torino` only. Cross-device comparison needed.
3. **6-Qubit Scale:** Effects may become more pronounced in larger GHZ states (9-12 qubits).
4. **Mechanistic Attribution:** Requires detailed gate-level noise models and hardware calibration data.

Future work should:

- Extend to other entangled states (W-states, cluster states).
- Perform time-resolved measurements to separate T_1 vs. gate errors.
- Develop noise maps from large-scale spatial asymmetry surveys.

5 Conclusion

We have demonstrated that multi-qubit entanglement decoheres *inhomogeneously* on NISQ devices, exhibiting measurable spatial structure dependent on hardware topology and circuit configuration. Our local asymmetry metric provides a quantitative probe of this effect, revealing that Configuration D produces 1.88× more asymmetry than Configuration B on `ibm_torino`.

These findings establish that quantum decoherence is not a spatially uniform process but carries hardware-specific fingerprints—analogous to how crystal defects

leave signatures in solid-state systems. As quantum processors scale to hundreds of qubits, spatial heterogeneity will become increasingly critical for understanding and mitigating noise.

Acknowledgments

This work was performed using IBM Quantum resources. We thank the IBM Quantum team for hardware access and technical support. All experiments were conducted via the Qiskit framework.

Data Availability

Raw experimental data and analysis scripts will be made available at `https://github.com/csaplard/ghz-asymmetry` following arXiv publication. Data available upon request at csaplar.d@gmail.com.

References

[1] M. A. Nielsen and I. L. Chuang, *Quantum Computation and Quantum Information*, Cambridge University Press (2010).

[2] D. M. Greenberger, M. A. Horne, and A. Zeilinger, "Going beyond Bell's theorem," in *Bell's Theorem, Quantum Theory and Conceptions of the Universe*, Springer (1989).

[3] J. Preskill, "Quantum Computing in the NISQ era and beyond," *Quantum* **2**, 79 (2018).

[4] F. Arute *et al.*, "Quantum supremacy using a programmable superconducting processor," *Nature* **574**, 505-510 (2019).

[5] D. C. McKay *et al.*, "Qiskit Backend Specifications for OpenQASM and OpenPulse Experiments," arXiv:1809.03452 (2018).

[6] S. Sheldon *et al.*, "Procedure for systematically tuning up cross-talk in the cross-resonance gate," *Phys. Rev. A* **93**, 060302(R) (2016).

[7] K. Wright *et al.*, "Benchmarking an 11-qubit quantum computer," *Nat. Commun.* **10**, 5464 (2019).

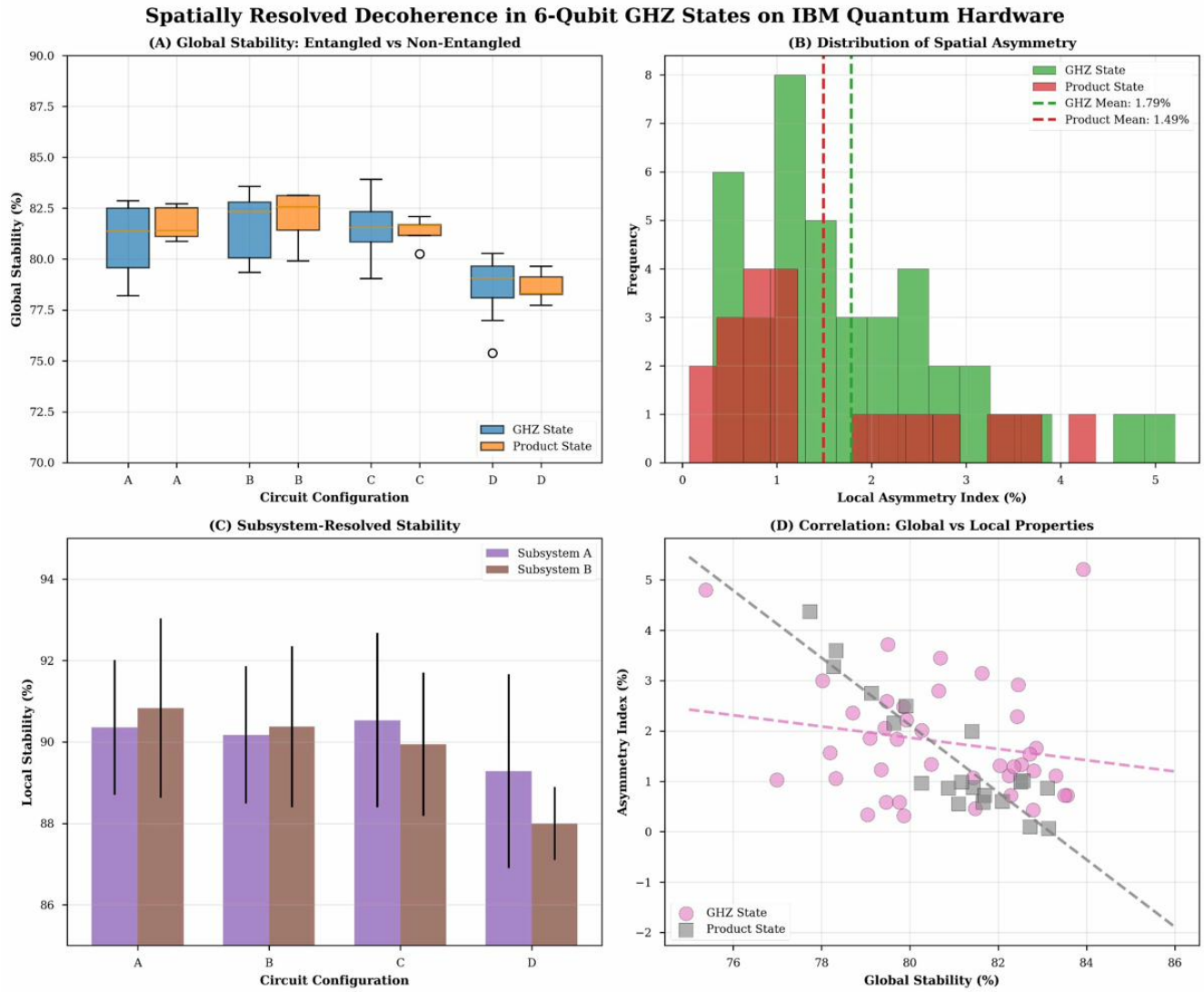

Figure 1: **Spatially Resolved Decoherence in 6-Qubit GHZ States.** (A) Global stability comparison between entangled GHZ states and non-entangled product states across four circuit configurations. (B) Distribution of local asymmetry index showing spatial inhomogeneity in decoherence. (C) Subsystem-resolved stability for subsystems A and B. (D) Correlation analysis between global stability and local asymmetry index.

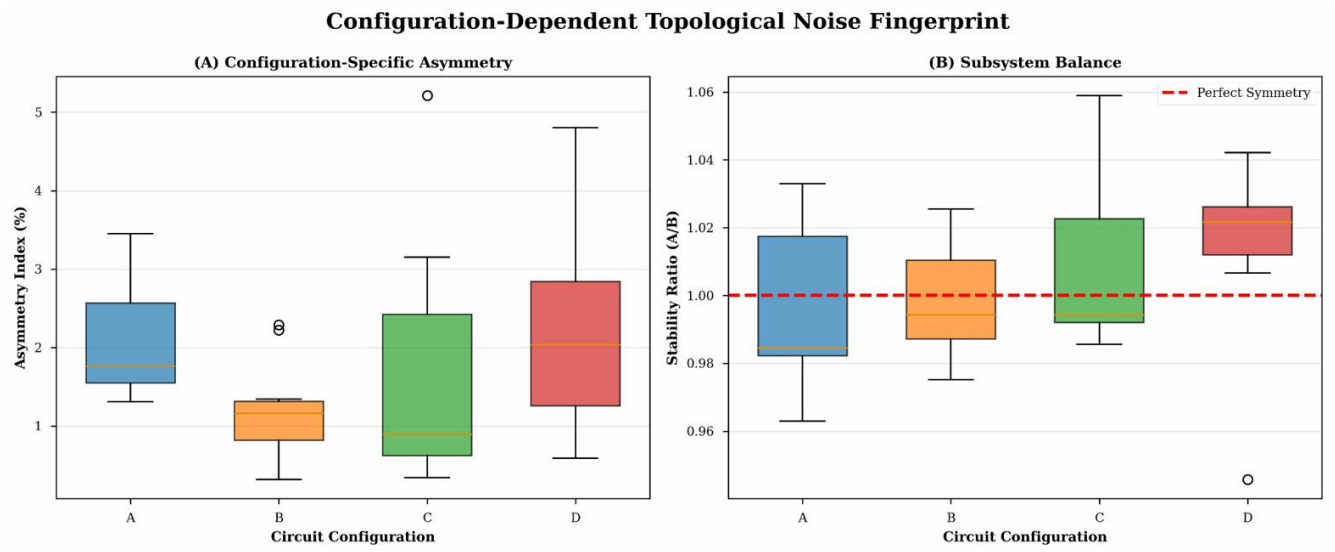

Figure 2: **Configuration-Dependent Topological Noise Fingerprint.** (A) Configuration-specific asymmetry showing 1.88× variation between Configuration B (lowest) and Configuration D (highest). (B) Subsystem balance ratio across all configurations, clustering near perfect symmetry (R=1.0) with small hardware-intrinsic bias.